# Low-crosstalk, filter-free, and secure WDM for optical inter-CubeSat communication using fluorescent fiber antennas

XINGCHEN YU, 1 CHEN CHEN, 1,5 D CUIWEI HE, 2,6 D ZIHAN WANG, 3 ZHIHONG ZENG, 1 DENGKE WANG, 1 MIN LIU, 1 AND HARALD HAAS4 D

**Abstract:** In this paper, a low-crosstalk, filter-free, and secure wavelength-division multiplexing (WDM) scheme based on fluorescent fiber antennas is proposed and demonstrated for optical inter-CubeSat communication (OICSC) systems. The integration of fluorescent fiber antennas in OICSC systems facilitates efficient WDM transmission to enhance the achievable data rate, owing to their inherent optical filtering capabilities. By selecting light-emitting diodes (LEDs) with distinctive emission wavelengths and fluorescent fiber antennas with the corresponding absorption wavelengths, physical WDM signal separation can be achieved to effectively minimize crosstalk at the receiver side. Furthermore, in order to address the performance imbalance across different wavelength channels and enhance transmission security, a chaotic two-dimensional pairwise coding (2D-PWC) scheme is further proposed for the WDM-OICSC system using fluorescent fiber antennas. Proof-of-concept experiments are conducted to verify the feasibility of using fluorescent fiber antennas to achieve low-crosstalk, filter-free, and secure WDM transmission in OICSC systems. Experimental results indicate that the proposed WDM-OICSC system using fluorescent fiber antennas exhibits a negligible crosstalk between two wavelength channels and the application of chaotic 2D-PWC can achieve enhanced bit error rate (BER) performance while ensuring transmission security. Specifically, a usable bandwidth of 18 MHz is obtained at the BER threshold of  $3.8 \times 10^{-3}$  using chaotic 2D-PWC, which corresponds to a 28.6% usable bandwidth extension compared with that without using PWC. It is also shown that an increasing number of fluorescent fiber bundles in each antenna consistently leads to a remarkable improvement in BER performance.

© 2025 Optica Publishing Group under the terms of the Optica Open Access Publishing Agreement

#### 1. Introduction

With the progress and development of society, people's demand for intelligence and information is getting higher and higher. Establishing communication networks across various locations on Earth is an intriguing objective that can be accomplished through the interconnection of satellites. The deployment of satellites in low-Earth orbits forms sensing and communication networks, providing Earth observation, disaster prevention and rural connectivity [1]. In recent years, the use of miniaturized satellites, known as CubeSats, has attracted much attention in satellite communication networks, due to the advantages of their numerous applications and low design-and-deployment cost [2]. Traditional inter-satellite communication typically leverages

<sup>&</sup>lt;sup>1</sup>School of Microelectronics and Communication Engineering, Chongqing University, Chongqing 400044,

<sup>&</sup>lt;sup>2</sup>School of Information Science, Japan Advanced Institute of Science and Technology, Ishikawa 923-1211, Japan

<sup>&</sup>lt;sup>3</sup>School of Cybersecurity, Chengdu University of Information Technology, Chengdu 610225, China

<sup>&</sup>lt;sup>4</sup>Department of Engineering, University of Cambridge, 9 JJ Thomson Avenue, Cambridge CB3 0FA, UK <sup>5</sup>c.chen@cqu.edu.cn

<sup>&</sup>lt;sup>6</sup>cuiweihe@jaist.ac.jp

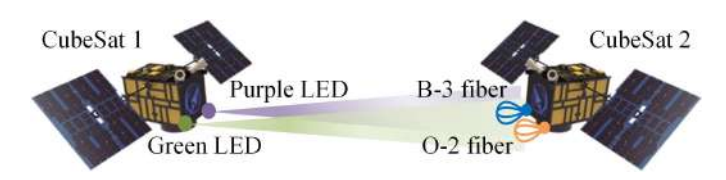
radio frequency (RF) or laser technologies to offer services. However, RF-based inter-satellite communication systems usually require large parabolic antennas, while laser-based inter-satellite communication systems generally need a high-precision acquisition, tracking and pointing (ATP) module. Therefore, both RF and laser technologies are not suitable for inter-CubeSat communication systems due to the limitations of size, mass, and power, as well as cost (SMaP-C) [3].

Compared with conventional RF and laser technologies, visible light communication (VLC) using light-emitting diodes (LEDs) has the advantages of small size, light weight, low power consumption and cost-effectiveness, which motivates the use of VLC with LEDs for inter-CubeSat communication systems under the SMaP-C limitations, and VLC-based optical inter-CubeSat communication (OICSC) has attracted great attention lately [4-6]. For example, heterogeneous optical network with novel modulation schemes and power control has been reported for OICSC systems to balance optical energy efficiency and spectral efficiency and further avoid inter-CubeSat interference [7,8]. Moreover, wavelength-division multiplexing (WDM) using light sources with multiple distinctive wavelengths has also been recognized as a key technology to improve the achievable data rate of satellite links [9–11]. In order to demultiplex the WDM signal at the receivers side, optical filters are generally adopted which can separate the individual wavelengths for subsequent signal detection. Nevertheless, the use of optical filters inevitably cause signal attenuation, and the WDM signal detector consisting of optical filters, optical lens and photo-detectors (PDs) usually has a bulky structure and a narrow field of view (FOV) due to the conservation of étendue [12]. To obtain both a high optical gain and a wide FOV with a compact structure, fluorescent fiber antennas have been considered as an efficient WDM demultiplexer for WDM-based VLC systems due to their inherent optical filtering capabilities [13]. Despite the appealing advantages of applying fluorescent fiber antennas for WDM demultiplexing, significant crosstalk might occur among different wavelength channels due to spectral overlap of the adopted LEDs and fluorescent fibers. Specifically, the green channel suffers non-negligible crosstalk from the blue channel in the established WDM-VLC system reported in [13], as the R-3 type fluorescent fiber absorbs both blue and green lights. To address the crosstalk issue, zero-forcing (ZF) equalization has been applied to remove the crosstalk in the green channel under the condition of amplified noise and reduced signal-to-noise ratio (SNR) performance. Furthermore, wavelength-domain pairwise coding (PWC) has been introduced in [13] to overcome the SNR imbalance issue among different wavelength channels. However, SNR imbalance occurs not only in the wavelength domain but also in the frequency domain among different subcarriers when using orthogonal frequency division multiplexing (OFDM) modulation. In addition, transmission security is also an important issue that should be considered when designing WDM schemes with wide-beam LEDs, especially for the security-sensitive applications such as satellite communications [14].

Aiming to address the crosstalk, SNR imbalance and security issues in WDM-OICSC systems, in this paper, we for the first time propose and demonstrate a low-crosstalk, filter-free and secure WDM scheme utilizing fluorescent fiber antennas. By properly selecting LEDs with distinctive emission wavelengths and fluorescent fiber antennas with the corresponding absorption wavelengths, the crosstalk among different wavelength channels can be effectively minimized at the receiver side. Moreover, a chaotic two-dimensional pairwise coding (2D-PWC) scheme is further proposed to overcome the SNR imbalance in both wavelength and frequency domains and enhance the transmission security simultaneously. The feasibility of using fluorescent fiber antennas to achieve low-crosstalk, filter-free and secure WDM transmission in OICSC systems is successfully verified by proof-of-concept experimental results.

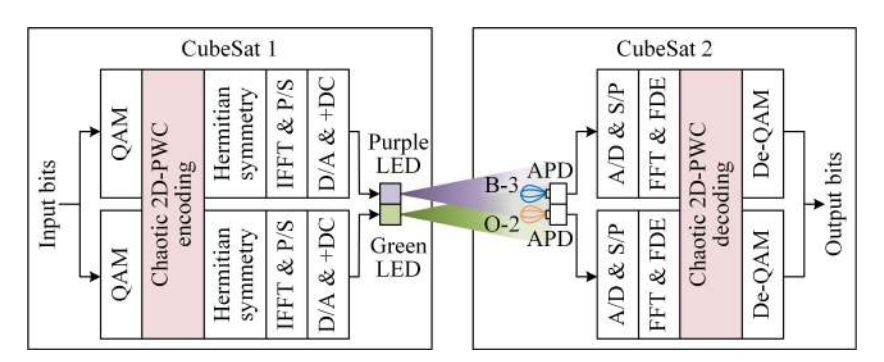
### 2. Principle

Figure 1 illustrates the general concept of a WDM-OICSC system using fluorescent fiber antennas to enable efficient WDM transmission between two CubeSats, where CubeSat 1 is equipped with two types of LEDs (i.e., a purple LED and a green LED) and CubeSat 2 is equipped with two types of antennas made of B-3 and O-2 fluorescent fibers which are commercially available products manufactured by Kuraray. Due to the inherent optical filtering capabilities of fluorescent fiber antennas, WDM demultiplexing can be efficiently performed without applying additional optical filters.



**Fig. 1.** Illustration of a WDM-OICSC system using fluorescent fiber antennas.

The schematic diagram of the WDM-OICSC system using fluorescent fiber antennas and chaotic 2D-PWC is depicted in Fig. 2. At CubeSat 1, as we can see, the input bits are first divided into two streams and then each stream is mapped into quadrature amplitude modulation (QAM) symbols with a specified modulation order. Subsequently, chaotic 2D-PWC encoding is conducted to address both the SNR imbalance and the security issues. After imposing Hermitian symmetry, inverse fast Fourier transform (IFFT) and parallel-to-serial (P/S) conversion, the obtained serial digital signal is converted into an analog signal via digital-to-analog (D/A) conversion and a direct current (DC) bias is further added to ensure the non-negativity of the analog signals. The resultant two signals are respectively used to modulate the purple and green LEDs so as to generate the transmitted WDM signal. At CubeSat 2, it can be seen that two antennas made of B-3 and O-2 fluorescent fibers are adopted to collect and demultiplex the WDM signal and each fluorescent fiber antenna is connected with an avalanche photodetector (APD) which converts the optical signal into an electrical signal. The principle of fluorescent fiber antennas will be introduced in Section 2.1. After analog-to-digital (A/D) conversion, serial-to-parallel (P/S) conversion, fast Fourier transform (FFT) and frequency-domain equalization (FDE), chaotic 2D-PWC decoding is executed accordingly. The detailed principle of chaotic 2D-PWC encoding and decoding will be discussed in Section 2.2. Finally, the output bits can be obtained through QAM demapping and bit combining.



**Fig. 2.** Schematic diagram of the WDM-OICSC system using fluorescent fiber antennas and chaotic 2D-PWC.

### 2.1. Fluorescent fiber antennas

The use of fluorescent fiber as antenna to enhance the performance of VLC systems has attracted much attention in recent years, due to its advantages of high optical gain, wide FOV and inherent optical filtering capability [15–17]. In this current work, we utilize B-3 and O-2 fluorescent fibers manufactured by Kuraray as two types of antennas to collect and demultiplex the WDM signal generated from a purple LED and a green LED.

Figure 3 show the optical spectra of the adopted fluorescent fibers and LEDs in the WDM-OICSC system. The absorption and emission spectra of the Kuraray B-3 fluorescent fiber are shown in Fig. 3(a), where it can be seen that the B-3 fluorescent fiber absorbs the light within the wavelength range from about 300 to 400 nm with an absorption peak wavelength of 350 nm, which is mainly corresponding to the purple light region. Moreover, the B-3 fluorescent fiber emits the light within the wavelength range from about 380 to 570 nm with an absorption peak wavelength of 350 nm, which is mainly corresponding to the blue light region. The absorption and emission spectra of the Kuraray O-2 fluorescent fiber are given in Fig. 3(b), where we can see that the O-2 fluorescent fiber mainly absorbs the green light and emits the orange light. The optical spectra of the selected purple and green LEDs are plotted in Fig. 3(c), where it is clear to see that the optical spectrum of the purple LED is mostly located within the absorption spectrum of the B-3 fluorescent fiber while the optical spectrum of the green LED is completely located within the absorption spectrum of the O-2 fluorescent fiber. Consequently, the crosstalk between the purple and green wavelength channels can be negligible and hence low-crosstalk and filter-free WDM transmission can be enabled in the WDM-OICSC system by employing B-3 and O-2 fluorescent fibers with purple and green LEDs.

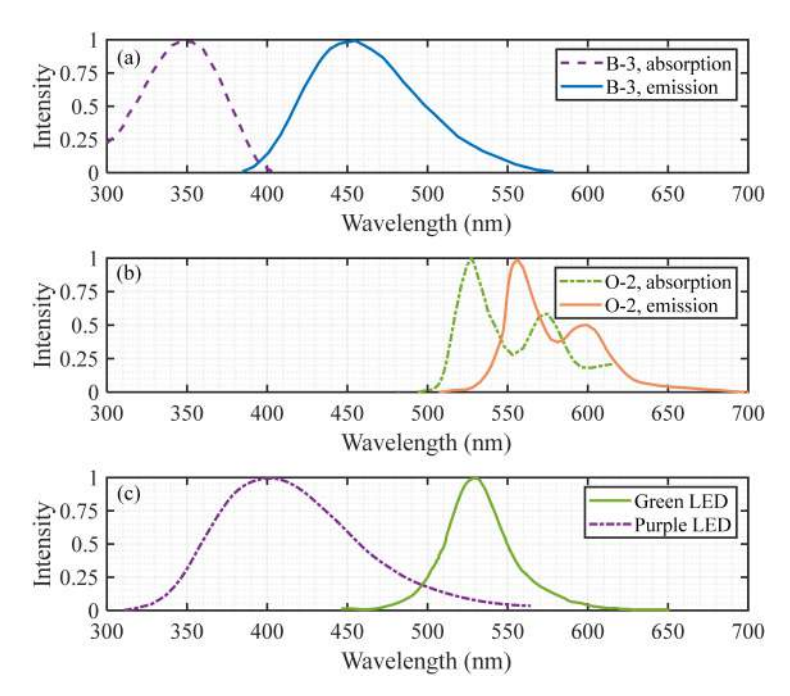


**Fig. 3.** Measured optical spectra of fluorescent fibers and LEDs: (a) absorption and emission spectra of the Kuraray B-3 fluorescent fiber, (b) absorption and emission spectra of the Kuraray O-2 fluorescent fiber, and (c) optical spectra of the purple and green LEDs.

Besides optical filtering, the photoluminescence (PL) lifetime of the fluorophores in fluorescent fiber antennas is another important parameter needs to be considered, which largely determines

the usable modulation bandwidth of the WDM channels. Fortunately, many organic and inorganic fluorophores typically have a short PL lifetime of several nanoseconds or less, which can enable relatively large modulation bandwidths and hence support high transmission data rates [18,19]. Figure 4 shows the measured frequency responses of the B-3 and O-2 fluorescent fibers, where the 10-dB modulation bandwidths of the B-3 and O-2 fluorescent fibers can reach 300 and 200 MHz, respectively. With the continuous development of fluorescent fiber technology, the usable modulation bandwidth of fluorescent fibers can be further substantially increased to support high-speed optical transmission for OICSC applications.

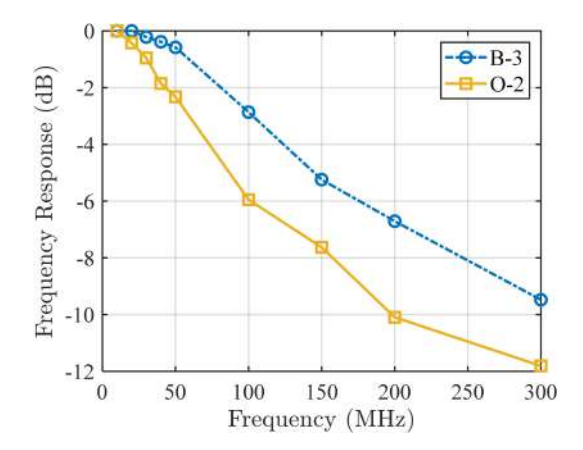


Fig. 4. The measured frequency responses of the B-3 and O-2 fluorescent fibers.

Fluorescent fiber antennas are generally made of polymethyl methacrylate (PMMA) materials, which have been shown to be beneficial for space applications due to its advantages of optical clarity, lightweight and mechanical strength [20]. Moreover, specific coatings such as anti-reflective coatings can be further added to enhance the durability of fluorescent optical fibers for OICSC applications in space environments.

# 2.2. Chaotic 2D-PWC

As an efficient approach to mitigate SNR imbalance, PWC has been introduced in various VLC systems which can be applied in the frequency, spatial, polarization or wavelength domain [13,21–24]. Moreover, PWC can also be jointly utilized in multiple domains to further balance the overall SNR performance of the VLC system [25,26]. Nevertheless, the pairing mechanism in PWC is usually straightforward and predictable, which might cause a security issue where the confidential information might be eavesdropped by unintended or unauthorized users.

To simultaneously address the SNR imbalance issue and the security issue for the WDM-OICSC system, a chaotic 2D-PWC scheme is further proposed. Figure 5 depicts the encoding process of the proposed chaotic 2D-PWC scheme, where PWC in performed jointly in both frequency and wavelength domains. As we can see, frequency-domain PWC (FD-PWC) is first performed with respect to each of the two wavelengths with a mirrored pairing mechanism, which involves angle rotation and pairwise in-phase(I) and quadrature (Q) interleaving. Assuming there are a total of N data subcarriers within each wavelength channel, the resultant data symbols  $s_i^{w_m}$  and  $s_{N-i+1}^{w_m}$  of the i-th subcarrier pair on the  $w_m$ -th wavelength channel with  $i = 1, 2, \ldots, N/2$  and m = 1, 2 after FD-PWC encoding are given by

$$\begin{cases} s_i^{w_m} = \Re(X_i^{w_m} e^{j\delta}) + j\Re(X_{N-i+1}^{w_m} e^{j\delta}) \\ s_{N-i+1}^{w_m} = \Im(X_i^{w_m} e^{j\delta}) + j\Im(X_{N-i+1}^{w_m} e^{j\delta}) \end{cases}$$
(1)

where  $X_n^{w_m}$  denotes the QAM symbols of the *n*-th subcarrier on the  $w_m$ -th wavelength channel with  $n=1,2,\ldots,N$ ,  $\Re(\cdot)$  and  $\Im(\cdot)$  respectively denote the operations to extract the I and Q components of a complex-valued input, and  $\delta$  is the rotation angle. According to [27], the rotation angle  $\delta$  can be generally assumed to be 45° to achieve satisfactory BER performance.

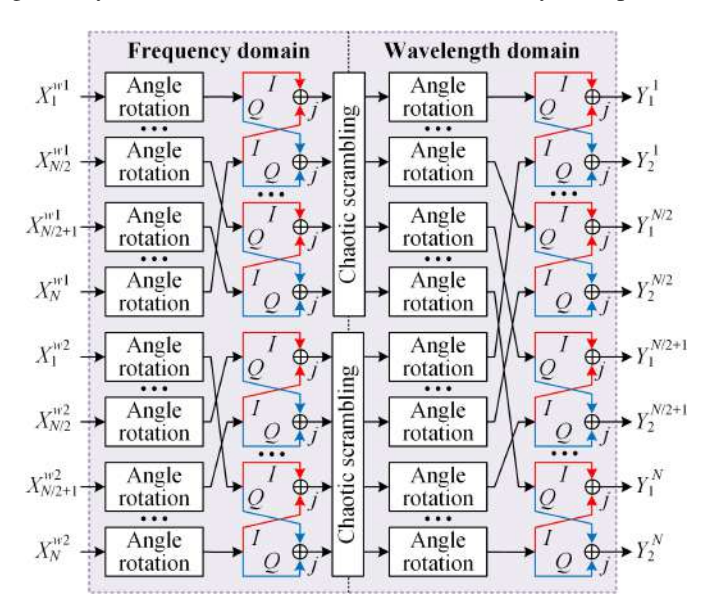


**Fig. 5.** Encoding process of the proposed chaotic 2D-PWC scheme.

Subsequently, chaotic scrambling is carried out with respect to each wavelength which encrypts the obtained symbol vector  $\mathbf{s}^{w_m} = [s_1^{w_m}, s_2^{w_m}, \dots, s_N^{w_m}]^T$  with  $(\cdot)^T$  denotes the transpose operation and m = 1, 2 by chaotically scrambling the positions of the elements in  $\mathbf{s}^{w_m}$ . The resultant symbol vector after performing chaotic scrambling can be represented by

$$\mathbf{r}^{w_m} = scr\left\{\mathbf{s}^{w_m}, \mathbf{p}_n^{w_m}\right\} \tag{2}$$

where  $scr \{\cdot, \cdot\}$  denotes the scrambling function and  $\mathbf{p}_n^{w_m}$  is the corresponding permutation vector. The scrambling function scrambles  $\mathbf{s}^{w_m}$  according to  $\mathbf{p}_n^{w_m}$  which indicates the new positions of the elements in the encrypted symbol vector  $\mathbf{r}^{w_m}$ .

As the permutation vector  $\mathbf{p}_n^{w_m}$  should be determined first before successfully performing chaotic scrambling, the piecewise linear chaotic map (PWLCM) is adopted [28], which is defined by

$$z_{t+1} = F_{\gamma}(z_t) = \begin{cases} z_t/\gamma, & 0 < z_t < \gamma \\ (z_t - \gamma)/(0.5 - \gamma), & \gamma \le z_t < 0.5 \\ F_{\gamma}(1 - z_t), & 0.5 \le z_t < 1 \end{cases}$$
 (3)

where  $0 < z_t < 1$  with t being the discrete time index. It has been shown that the chaotic system defined by Eq. (3) falls into the chaotic domain when  $0 < \gamma < 0.5$  [28]. Consequently, the permutation vector  $\mathbf{p}_n^{w_m}$  with m = 1, 2 can be obtained by using the state  $z_t$  as follows:

$$\mathbf{p}_{n}^{w_{1}} = sort \left\{ [z_{1}, z_{2}, \dots z_{N}]^{T} \right\}$$
(4)

$$\mathbf{p}_{n}^{w_{2}} = sort \left\{ \left[ z_{N+1}, z_{N+2}, \dots z_{2N} \right]^{T} \right\}$$
 (5)

where  $sort \{\cdot\}$  denotes the sorting function which returns the index vector of the elements of the input vector by sorting these elements in a descending order.

Afterwards, it can be seen that wavelength-domain PWC (WD-PWC) is further performed with respect to the overall encrypted symbol vector  $\mathbf{u} = [\mathbf{r}^{w_1}; \mathbf{r}^{w_2}] = [u_1, u_2, \dots, u_{2N}]^T$  with a sequential pairing mechanism. Finally, the resultant data symbols  $Y_1^n$  and  $Y_2^n$  of the *n*-th subcarrier pair after WD-PWC encoding are given by

$$\begin{cases} Y_1^n = \Re(u_n e^{j\delta}) + j\Re(u_{N+n} e^{j\delta}) \\ Y_2^n = \Im(u_n e^{j\delta}) + j\Im(u_{N+n} e^{j\delta}) \end{cases}$$
(6)

where n = 1, 2, ..., N and the rotation angle  $\delta$  is also assumed to be 45°.

For the decoding of chaotic 2D-PWC, its process is exactly the inverse process of chaotic 2D-PWC encoding, where the only difference is that the corresponding rotation angles are set to be  $-45^{\circ}$ . Hence, the schematic of chaotic 2D-PWC decoding is not provided here for the sake of brevity. It should also be noted that the chaotic descrambling during chaotic 2D-PWC decoding follows the inverse process of the chaotic scrambling during chaotic 2D-PWC encoding where the same the permutation vector  $\mathbf{p}_n^{w_m}$  is utilized to realize chaotic descrambling. Specifically, since both  $z_0$  and  $\gamma$  can be set as the shared security key during chaotic scrambling and descrambling the key space of the adopted chaotic encryption scheme can be calculated as follows. Given  $0 < z_0 < 1$  and  $0 < \gamma < 0.5$ , the key space for a 64-bit doubleprecision number with the computational precision of approximately  $10^{-15}$  is calculated by  $[(1-0) \times 10^{15}] \times [(0.5-0) \times 10^{15}] = 5 \times 10^{29}$ .

#### 3. Experiment setup and results

In this section, proof-of-concept experiments within the lab environment are conducted verify the feasibility of applying fluorescent fiber antennas and chaotic 2D-PWC in WDM-OICSC systems. The experimental setup of a proof-of-concept WDM-OICSC system using fluorescent fiber antennas is depicted in Fig. 6, where the transmitted signals are first generated offline using MATLAB. Then, the digital signals are uploaded into a two-channel arbitrary waveform generator (AWG, Tektronix AFG31102) where the sampling rates of two channels are both set to 50 MSa/s. Subsequently, the AWG output signals with respect to the green and purple LEDs are respectively combined with DC bias voltages of 2.5 V and 4 V via two bias tees (bias-T, Mini-circuit ZFBT-6GW+). The resultant combined signals are then used to drive the green and purple LEDs to generate the WDM signal. At the receiver side, two antennas made of Kuraray O-2 and B-3 fluorescent fibers are adopted to collect and demultiplex the WDM signal. Each fluorescent fiber antenna is connected with a commercial APD module (APD, Hamamatsu C12702-12). Finally, the detected electrical analog signals are captured by a two-channel oscilloscope (DSO, Tektronix MDO32) with a sampling rate of 200 MSa/s and the digitized signals are further processed offline using MATLAB.

In the experiments, each fluorescent fiber antenna can consist of multiple fiber bundles and each fiber bundle has a length of 20 cm. Moreover, the IFFT/FFT size during OFDM modulation/demodulation is 256 and the adopted constellation is 4QAM for both green and purple channels. The effective OFDM signal bandwidth is adjusted by changing the number of data subcarriers before IFFT in the following experiments. The inset of Fig. 6 shows the photo of the established experimental testbed in a lab environment.

Figure 7 plots the measured channel responses of the WDM-OICSC system using fluorescent fiber antennas. It can be observed that the response of the green channel using O-2 fluorescent fiber antenna is at least 20-dB higher than that using B-3 fluorescent fiber antenna, which is mainly due to the fact that B-3 fluorescent fiber antenna can barely absorb the green light as shown in Fig. 3(a). Moreover, the response of the purple channel using B-3 fluorescent fiber antenna is about 10-dB higher than that using O-2 fluorescent fiber antenna, which is because O-2 fluorescent fiber antenna can still slightly absorb the purple light as can be seen from Fig. 3(b). The measured channel responses in Fig. 7 clearly verify that the crosstalk between green and

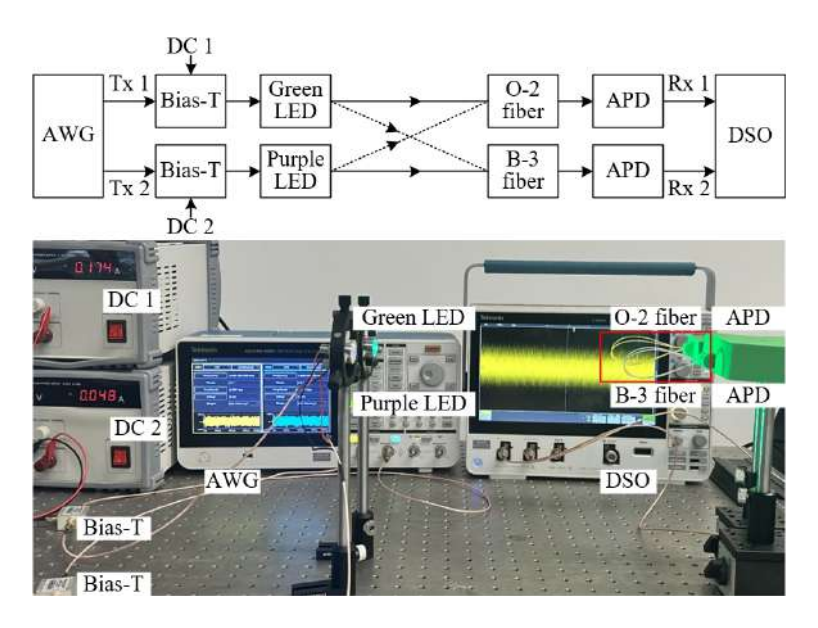
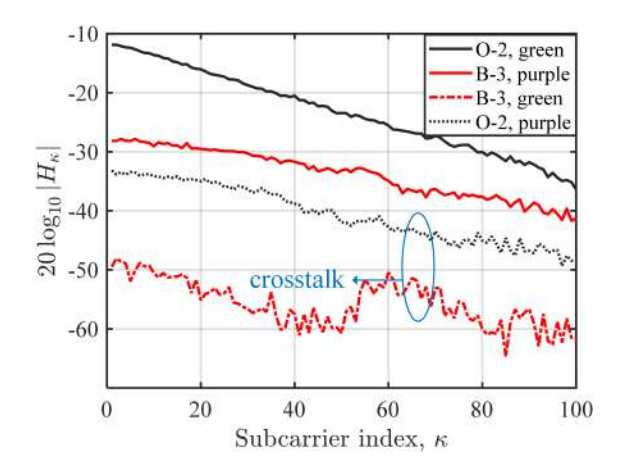


Fig. 6. Experimental setup of the WDM-OICSC system using fluorescent fiber antennas.

purple channels is almost negligible. Hence, crosstalk equalization is not required in the proposed WDM-OICSC system using fluorescent fiber antennas and the demultiplexed signals can be directly used for demodulation.



**Fig. 7.** Measured channel responses of the WDM-OICSC system using fluorescent fiber antennas.

Figure 8 shows the experimental BER versus effective signal bandwidth for different PWC schemes, where each fluorescent fiber antenna consists of two fiber bundles. As we can see, the BER gradually increases with the increase of bandwidth for all the considered schemes, which is mainly because of the gradual reduction of the received SNR due to bandwidth extension and low-pass effect. The WDM-OICSC system without using PWC exhibits the highest BER and the usable bandwidth at the 7% forward error correction (FEC) coding threshold of BER =  $3.8 \times 10^{-3}$  is about 14 MHz. In contrast, the use of PWC coding can efficiently improve the overall BER performance of the system. Specifically, one-dimensional PWC (1D-PWC) schemes including WD-PWC and FD-PWC have nearly the same BER performance, both achieving a

usable bandwidth of about 17 MHz at BER =  $3.8 \times 10^{-3}$ . Moreover, 2D-PWC obtains the largest usable bandwidth of about 19 MHz at BER =  $3.8 \times 10^{-3}$ , which is corresponding to a usable bandwidth extension of 35.7% in comparison to that without using PWC. When the proposed chaotic 2D-PWC scheme is employed, its BER performance is slightly worse than that of 2D-PWC, which is due to the introduction of additional chaotic scrambling processes during 2D-PWC encoding, making the subcarrier pairing less balanced and hence slightly reducing the capability of SNR imbalance mitigation. Nevertheless, a usable bandwidth of about 18 MHz at BER =  $3.8 \times 10^{-3}$  can still be obtained by chaotic 2D-PWC, which is corresponding to a 28.6% usable bandwidth extension compared with that without using PWC. In addition, as shown in the inset in Fig. 8, the BER of the system using chaotic 2D-PWC without the correct key is always around 0.3 for different bandwidths, which indicates that the eavesdropper cannot get any useful information from the received OFDM signal and hence successfully verifies the security of the proposed WDM-OICSC system.

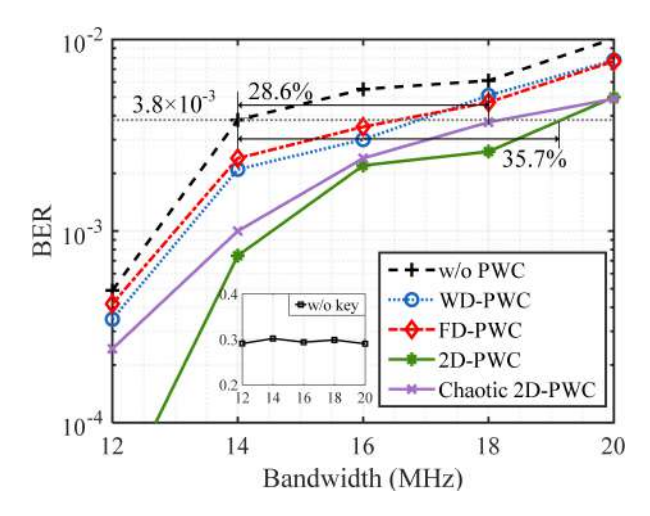
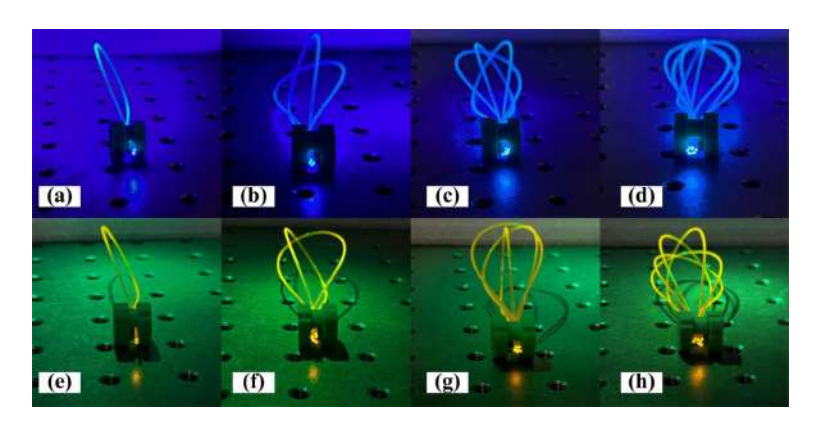


Fig. 8. Experimental BER vs. signal bandwidth for different PWC schemes.

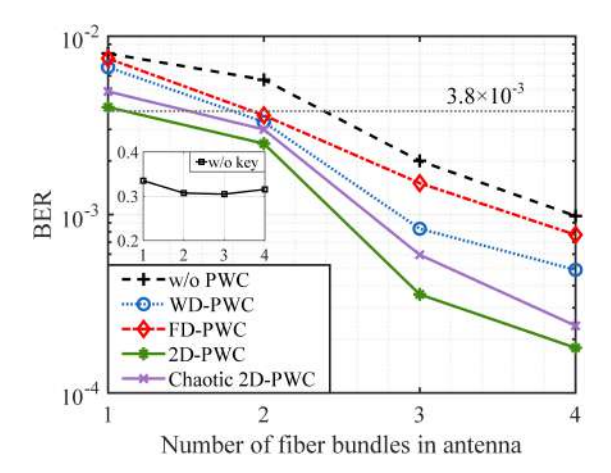
When fluorescent fibers are used as optical antennas in the WDM-OICSC system, the optical power of the collected light highly depends on the length of the fiber and one fluorescent fiber antenna can consist of multiple fiber bundles. Figure 9 depicts the photos of fluorescent fiber antennas using B-3 and O-2 fluorescent fibers with different numbers of bundles per antenna. It is evident to see that an increase in the number of fiber bundles per antenna results in a higher photon count reaching the receiving end of the antenna. Moreover, the adoption of an approximate spherical fiber winding technique is contemplated, which aims to maximize the effective receiving area of the fiber to capture the incident photons. This geometric design enhances the capacity of the fiber to absorb photons by expanding the surface area available for interaction with the incoming light.

Figure 10 shows the experimental BER versus number of fiber bundles in antenna for different PWC schemes, where the signal bandwidth is set to 16 MHz. It can be observed that the BER is gradually reduced when each antenna is made of a larger number of fiber bundles for all the considered schemes. Particularly, for the case without applying PWC coding, the BER is reduced from  $5.7 \times 10^{-3}$  to  $9.8 \times 10^{-4}$  when the number of fiber bundles in antenna is increased from 2 to 4. Moreover, WD-PWC outperforms FD-PWC in terms of BER performance when the number of fiber bundles in antenna reaches 3 and 4, which is mainly due to the enlarged SNR imbalance between two wavelength channels when the fluorescent fiber antennas can absorb more incident photons. Similarly, the best BER performance is obtained by 2D-PWC, and the proposed chaotic



**Fig. 9.** Photos of fluorescent fiber antennas: (a) B-3, one bundle, (b) B-3, two bundles, (c) B-3, three bundles, (d) B-3, four bundles, (e) O-2, one bundle, (f) O-2, two bundles, (g) O-2, three bundles, and (h) O-2, four bundles.

2D-PWC can not only achieve a comparable BER performance as 2D-PWC but also guarantee the security of the overall system. The inset in Fig. 10 demonstrates that the system has a BER of around 0.3 for different numbers of fiber bundles in antenna when the eavesdropper does not have the correct key to perform chaotic descrambling.



**Fig. 10.** Experimental BER vs. number of fiber bundles in antenna for different PWC schemes.

#### 4. Conclusions

In this paper, we have proposed and experimentally demonstrated a low-crosstalk, filter-free, and secure WDM scheme by using fluorescent fiber antennas for OICSC systems. These antennas are employed in supporting efficient WDM transmission which can significantly boost the achievable data rate of the OICSC system, because they are capable of optical filtering. Moreover, physical separation of WDM signals can be implemented to significantly reduce crosstalk at the receiver side by properly designing the optical WDM transmitter and the optical receiver with fluorescent fiber antennas. To further improve the system performance, chaotic 2D-PWC has also been proposed to simultaneously mitigate SNR imbalance between two wavelength channels and enhance the security of the overall system. Experimental results successfully verify the feasibility

of the proposed WDM-OICSC system using fluorescent fiber antennas with chaotic 2D-PWC. In conclusion, the combination of fluorescent fiber antennas and chaotic 2D-PWC can be a promising candidate for future high-speed and secure WDM-OICSC systems.

In our future work, omnidirectional fluorescent fiber antennas will be designed to address the mobility issue of CubeSats in OICSC systems. Moreover, large-bandwidth LED transmitters will be utilized in the proposed WDM-OICSC system to address the bandwidth limitation issue.

**Funding.** National Natural Science Foundation of China (62271091); Fundamental Research Funds for the Central Universities (2024CDJXY020).

**Disclosures.** The authors declare no conflicts of interest.

**Data availability.** The data underlying the results presented in this paper are not publicly available at this time but may be obtained from the authors upon reasonable request.

#### References

- O. Kodheli, E. Lagunas, N. Maturo, et al., "Satellite communications in the new space era: A survey and future challenges," IEEE Commun. Surv. Tutorials 23(1), 70–109 (2021).
- N. Saeed, A. Elzanaty, H. Almorad, et al., "CubeSat communications: Recent advances and future challenges," IEEE Commun. Surv. Tutorials 22(3), 1839–1862 (2020).
- G. Wang, F. Yang, J. Song, et al., "Free space optical communication for inter-satellite link: Architecture, potentials and trends," IEEE Commun. Mag. 62(3), 110–116 (2024).
- L. Wood, W. Ivancic, and K.-P. Dörpelkus, "Using light-emitting diodes for intersatellite links," in *IEEE Aerospace Conference*, (IEEE, 2010), pp. 1–6.
- D. N. Amanor, W. W. Edmonson, and F. Afghah, "Intersatellite communication system based on visible light," IEEE Trans. Aerosp. Electron. Syst. 54(6), 2888–2899 (2018).
- A. Anzagira, W. W. Edmonson, and D. N. Amanor, "LED-based visible light intersatellite communication for distributed space systems," IEEE J. Miniat. Air Space Syst. 2(3), 140–147 (2021).
- X. Huang, P. Chen, and X. Xia, "Heterogeneous optical network and power allocation scheme for inter-CubeSat communication," Opt. Lett. 49(5), 1213–1216 (2024).
- 8. X. Huang, M. Peng, and J. Song, "Heterogeneous network for inter-NanoSat communication with novel modulation schemes and power control," IEEE Commun. Lett. 28(4), 897–901 (2024).
- L. Gu, F. Zhao, Z. Shi, et al., "Four-channel coarse WDM for inter-and intra-satellite optical communications," Opt. Laser Technol. 37(7), 551–554 (2005).
- 10. M. R. Djellouli, S. A. Chouakri, and A. Ghaz, "OWC inter satellite link throughput improvement based on WDM architecture," in *International Conference on Advanced Electrical Engineering (ICAEE)*, (2022), pp. 1–6.
- 11. E. Ciaramella and G. Cossu, "Nonlinear fiber effects in ultra-high power 10× 10 Gbit/s WDM-IM free-space systems for satellite links," Opt. Express 32(5), 7959–7968 (2024).
- 12. C. He and C. Chen, "A review of advanced transceiver technologies in visible light communications," in *Photonics*, vol. 10 (MDPI, 2023), p. 648.
- 13. C. He, Y. Tang, C. Chen, *et al.*, "Wavelength division multiplexing in visible light communications using fluorescent fiber antennas," J. Lightwave Technol. **42**(10), 3725–3735 (2024).
- P. Tedeschi, S. Sciancalepore, and R. Di Pietro, "Satellite-based communications security: A survey of threats, solutions, and research challenges," Comput. Networks 216, 109246 (2022).
- 15. W. Ali, Z. Ahmed, W. Matthews, *et al.*, "The impact of the length of fluorescent fiber concentrators on the performance of VLC receivers," IEEE Photonics Technol. Lett. **33**(24), 1451–1454 (2021).
- C. He, Y. Lim, and H. Murata, "Study of using different colors of fluorescent fibers as optical antennas in white LED based-visible light communications," Opt. Express 31(3), 4015–4028 (2023).
- C. He and S. Collins, "A two-stage fluorescent antenna for visible light communication uplinks," IEEE Photonics Technol. Lett. 35(21), 1190–1193 (2023).
- W. Ali, P. P. Manousiadis, D. C. O'Brien, et al., "A Gigabit VLC receiver that incorporates a fluorescent antenna and a SiPM," J. Lightwave Technol. 40(16), 5369–5375 (2022).
- M. Portnoi, P. A. Haigh, T. J. Macdonald, et al., "Bandwidth limits of luminescent solar concentrators as detectors in free-space optical communication systems," Light: Sci. Appl. 10(1), 3 (2021).
- S. Link, X. Huang, C. Fernandez-Pello, et al., "The effect of gravity on flame spread over PMMA cylinders," Sci. Rep. 8(1), 120 (2018).
- J. He and J. Shi, "An enhanced adaptive scheme with pairwise coding for OFDM-VLC system," IEEE Photonics Technol. Lett. 30(13), 1254–1257 (2018).
- 22. J. Shi, J. He, Y. Hong, *et al.*, "Performance-enhanced NOMA-VLC using subcarrier pairwise coding," Opt. Commun. **450**, 141–146 (2019).
- B. Deng, J. Wang, Z. Wang, et al., "Polarization multiplexing based UOWC systems under bubble turbulence," J. Lightwave Technol. 41(17), 5588–5598 (2023).

- 24. Y. Nie, C. Chen, Z. Zeng, *et al.*, "Multi-mode index modulation aided multi-band CAP with balanced pairwise coding for bandlimited VLC systems," J. Lightwave Technol. **43**(5), 2053–2066 (2025).
- H. G. Olanrewaju, J. Thompson, and W. O. Popoola, "Pairwise coding for MIMO-OFDM visible light communication," IEEE Trans. Wireless Commun. 19(2), 1210–1220 (2020).
- 26. J. Wang, C. Chen, B. Deng, *et al.*, "Enhancing underwater VLC with spatial division transmission and pairwise coding," Opt. Express **31**(10), 16812–16832 (2023).
- 27. C. Zhu, B. Song, B. Corcoran, *et al.*, "Improved polarization dependent loss tolerance for polarization multiplexed coherent optical systems by polarization pairwise coding," Opt. Express **23**(21), 27434–27447 (2015).
- Y. Yang, C. Chen, W. Zhang, et al., "Secure and private NOMA VLC using OFDM with two-level chaotic encryption," Opt. Express 26(26), 34031–34042 (2018).